Presented at: ASME International Mechanical Engineering Congress and Exposition
'Symposium on Nonlinear and Stochastic Dynamics'
Chicago, Illinois
November 13-18, 1994

STEADY-STATE DYNAMIC BEHAVIOR OF AN AUXILIARY BEARING SUPPORTED ROTOR SYSTEM

Huajun Xie and George T. Flowers

Department of Mechanical Engineering
Auburn University
Auburn, Alabama

Charles Lawrence

NASA Lewis Research Center
Cleveland, Ohio

ABSTRACT

This paper investigates the steady-state responses of a rotor system supported by auxiliary bearings in which there is a clearance between the rotor and the inner race of the bearing. A simulation model based upon the rotor of a production jet engine is developed and its steady-state behavior is explored over a wide range of operating conditions for various parametric configurations. Specifically, the influence of rotor imbalance, support stiffness and damping is studied. It is found that imbalance may change the rotor responses dramatically in terms of frequency contents at certain operating speeds. Subharmonic responses of 2nd order through 10th order are all observed except the 9th order. Chaotic phenomenon is also observed. Jump phenomena (or double-valued responses) of both hard-spring type and soft-spring type are shown to occur at low operating speeds for systems with low auxiliary bearing damping or large clearance even with relatively small imbalance. The effect of friction between the shaft and the inner race of the bearing is also discussed.

NOMENCLATURE

C_B = auxiliary bearing support damping, lb.s^2/in.
$C_{B\psi}$ = auxiliary bearing torsional damping, lb.in.s
F_n = normal force, lb
F_t = friction force, lb
$\mathbf{F}_X$ = external force vector acting on the rotor in X direction
$\mathbf{F}_Y$ = external force vector acting on the rotor in Y direction
$\mathbf{I}_a$ = rotor inertia matrix
J_B = moment of inertia of auxiliary bearing, lb.in.s^2
K_B = auxiliary bearing support stiffness, lb/in.
K_C = contact stiffness, lb/in.
M_B = auxiliary bearing mass, lb.s^2/in.
M_k = mass of kth rotor element, lb.s^2/in.
N = total number of modes considered
$NB1$ = node number at auxiliary bearing #1
$NB2$ = node number at auxiliary bearing #2
$\mathbf{Q}_X$ = rotor modal coordinate vector in X direction
$\mathbf{Q}_Y$ = rotor modal coordinate vector in Y direction
R_B = radius of auxiliary bearing bore, in.
R_m = radius of auxiliary bearing pitch, in.
R_R = radius of rotor journal, in.
$\mathbf{X}_R$ = rotor physical coordinate vector in X direction
$\mathbf{Y}_R$ = rotor physical coordinate vector in Y direction
e = rotor imbalance eccentricity, in.
g = gravitational acceleration, in./s^2
t = time, s
Δ = deformation at the contact point, in.
$\mathbf{\Gamma} = \mathbf{\Psi}^T \mathbf{I}_a \mathbf{\Psi}$
$\mathbf{\Psi}$ = rotor free-free modal rotation matrix
Ω = rotor operating speed, rad/s
$\mathbf{\Phi}$ = rotor free-free modal displacement matrix
$\delta = R_B - R_R$, auxiliary bearing clearance, in.
μ = dynamic friction coefficient
μ_ψ = rolling friction coefficient
ψ_B = angular displacement of auxiliary bearing inner-race
ζ = modal damping coefficient

INTRODUCTION

One of the most innovative developments in the turbomachinery field involves the use of active magnetic bearings (AMB) for rotor support. This technology provides the potential for significant improvements in the dynamic behavior of rotor systems, allowing for loading, eccentricity, shaft position and vibration to be continuously monitored and controlled. In order to protect the soft iron cores of the magnetic bearings and to provide rotor support in the event of failure of the bearing or during an overload situation, backup (or auxiliary) bearings, with a clearance between the rotor and the inner race of the bearing, are usually included in the rotor design. This clearance introduces a nonlinear dynamical feature which may significantly impact the behavior of the rotor.

Magnetic bearing systems appear to provide particularly great promise for use in aerospace applications. There are active programs at many of the major jet engine manufacturers to develop engines supported by magnetic bearings. Safety is a major concerns in any aeronautical design. Toward this end, it is desirable to design the rotor system to take maximum advantage of the backup bearings and use them as true auxiliary bearings to provide support during critical situations in a safe and consistent manner. An important concern in this regard is the dynamic behavior of the rotor when it comes into contact with the auxiliary bearing. If safe and effective operation of the engine is to be ensured during these periods, it is essential that designers have a very good understanding of the steady–state dynamics of rotor systems with clearance effects.

There are a number of studies in the literature concerned with the dynamics of rotors with clearance effects. Yamamoto (1954) conducted a systematic study of rotor responses involving bearing clearance effects. Black (1968) studied the rotor/stator interaction with a clearance. He concluded that rotor/stator interactions may occur in a variety of forms and circumstances, including jump phenomena. Ehrich (1966) reported the first identification of a second order subharmonic vibration phenomenon in a rotor system associated with bearing clearance (1966). Bently (1974) published experimental observations of second and third order subharmonic vibration in a rotor system. Later, Muszynska (1984) cited the occurrence of second, third, and fourth order subharmonic responses in a rotor rubbing case and Ehrich (1988 and 1991) observed eighth and ninth order subharmonic vibration as well as chaotic vibration in a high speed turbomachine. Childs (1979 and 1982) published two papers to explain the mechanism for the second and third order subharmonic responses noted above. He stated, with great insight, that " motion due to nonsymmetric clearance effects is a fractional–frequency phenomenon."

While those studies have greatly enhanced the understanding of clearance effects on rotor dynamics, a more detailed understanding of the dynamical behavior of such systems is needed. The perspective of much of this earlier work is that the clearance exists as a result of manufacturing error or misfitting. That is, it is due to an abnormal situation. However, in a rotor system fitted with magnetic bearings and auxiliary bearings, the clearance becomes a design parameter rather than an irregularity. From this point of view, it is important to develop a detailed quantitative understanding of the dynamic responses that are to be expected. Such knowledge will provide guidelines for the selection of auxiliary bearing parameters.

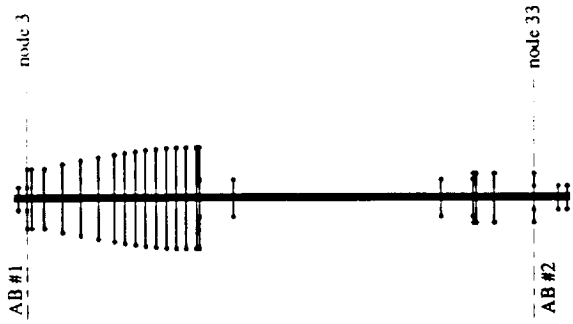

FIG. 1 DIAGRAM OF THE FEM ROTOR MODEL

It seems that there have been little work to date that is specifically concerned with auxiliary bearings in magnetic bearing supported rotor systems. Two papers that are directly related to research on auxiliary bearings were both focused on transient responses. Gelin et al. (1990) studied the transient dynamic behavior of rotors on auxiliary bearings during the coast down. Ishii and Kirk (1991) investigated the transient responses of a flexible rotor during the rotor drop after the magnetic bearings become inactive. In both papers, idealized rotor models are used and it is assumed that once the magnetic bearings fail, the torque is cut off and consequently the rotor speed approaches zero.

In this paper, simulation results are presented for a complex rotor system supported by auxiliary bearings with clearance at each end of the rotor. This work is specifically concerned with systems in which the clearances are quite small (on the order of a few mils), which is appropriate for jet engine applications in which the backup bearing is acting to provide rotor support on a consistent basis. The influence of rotor imbalance, support stiffness and support damping are investigated using direct numerical integration of the governing equations of motion and the harmonic balance method. Some insights are obtained with regard to the frequency and amplitude behavior of the steady–state vibration of such a system.

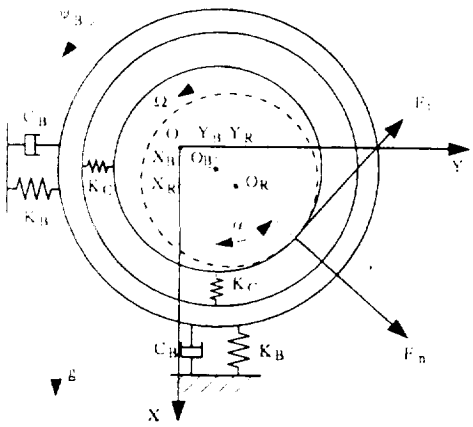

FIG. 2 AUXILIARY BEARING MODEL

SIMULATION MODEL

The rotor is modelled using free–free normal mode shapes and natural frequencies obtained through finite element analysis. The model data is representative for the rotor of a jet engine. Fig. 1 shows a schematic diagram of the FEM rotor model. Parametric information about the model is listed in Table 1. The torsional motion of the shaft is not considered in this paper. Using state space representation and modal coordinates, the equations of motion for the rotor are expressed as

$$\ddot{\mathbf{Q}}_X + 2\zeta\omega_n\dot{\mathbf{Q}}_X + \Omega\mathbf{\Gamma}\dot{\mathbf{Q}}_Y + \omega_n^2\mathbf{Q}_X + 2\Omega\zeta\omega_n\mathbf{Q}_Y = \mathbf{\Phi}^T\mathbf{F}_X, \tag{1.a}$$

$$\ddot{\mathbf{Q}}_Y + 2\zeta\omega_n\dot{\mathbf{Q}}_Y - \Omega\mathbf{\Gamma}\dot{\mathbf{Q}}_X + \omega_n^2\mathbf{Q}_Y - 2\Omega\zeta\omega_n\mathbf{Q}_X = \mathbf{\Phi}^T\mathbf{F}_Y, \tag{1.b}$$

where

$$\mathbf{F}_X = \{F_{X1}, F_{X2}, \ldots, F_{Xm}\}^{-1},$$
$$\mathbf{F}_Y = \{F_{Y1}, F_{Y2}, \ldots, F_{Ym}\}^{-1},$$
$$\mathbf{Q}_X = \mathbf{\Phi}^{-1}\mathbf{X}_R,$$
$$\mathbf{Q}_Y = \mathbf{\Phi}^{-1}\mathbf{Y}_R,$$

with

$$\mathbf{X}_R = \{X_{R1}, X_{R2}, \ldots, X_{Rm}\}^{-1},$$
$$\mathbf{Y}_R = \{Y_{R1}, Y_{R2}, \ldots, Y_{Rm}\}^{-1}.$$

(m = total number of nodes)

The physical displacements of the rotor at the two auxiliary bearing locations can be obtained using the following coordinate transformation:

$$X_{Rk} = \sum_{i=1}^{N} \Phi_{ik} Q_{Xi}, \qquad Y_{Rk} = \sum_{i=1}^{N} \Phi_{ik} Q_{Yi}, \qquad (k = NB1, NB2)$$

The equations of motion for the auxiliary bearings are derived using the model shown in Fig. 2

$$M_{Bk}\ddot{X}_{Bk} + C_{Bk}\dot{X}_{Bk} + K_{Bk}X_{Bk} = F_{nk}\cos\alpha_k - F_{tk}\sin\alpha_k + M_{Bk}\,g, \tag{2.a}$$

$$M_{Bk}\ddot{Y}_{Bk} + C_{Bk}\dot{Y}_{Bk} + K_{Bk}Y_{Bk} = F_{nk}\sin\alpha_k + F_{tk}\cos\alpha_k, \tag{2.b}$$

$$J_{Bk}\ddot{\psi}_{Bk} + C_{B\psi k}\dot{\psi}_{Bk} = F_{tk}R_{Bk} - \mu_\psi F_{nk}R_{mk}, \tag{2.c}$$

where

$$\alpha_k = tan^{-1}\frac{Y_{Rk} - Y_{Bk}}{X_{Rk} - X_{Bk}}. \qquad (k = NB1, NB2)$$

At this point, the rotor and the back-up bearings appear to be uncoupled. However, the force vectors $\mathbf{F}_X$ and $\mathbf{F}_Y$ on the right hand sides of equations (1) are partially due to rotor/auxiliary bearing interaction. In fact, we have

$$F_{Xk} = -F_{nk}\cos\alpha_k + F_{tk}\sin\alpha_k + M_k\,g + M_k\,e\,\Omega^2\cos(\Omega t),$$
$$F_{Yk} = -F_{nk}\sin\alpha_k - F_{tk}\cos\alpha_k + M_k\,e\,\Omega^2\sin(\Omega t).$$

The rotor/bearing interaction is represented with the normal force F_{nk}

$$F_{nk} = \begin{cases} K_C\delta_k, & \Delta_k < 0, \\ 0, & \Delta_k \geq 0, \end{cases} \tag{3.a}$$

where

$$\Delta_k = (X_{Rk} - X_{Bk})\cos\alpha_k + (Y_{Rk} - Y_{Bk})\sin\alpha_k - \delta_k$$

and the Coulomb friction force F_{tk}. As long as there exists slip at the contact point, the friction force obeys

$$F_{tk} = \mu\,F_{nk}. \tag{3.b}$$

However, when there is no slip at the contact point, the friction forces are solved from equations (1) and (2) using

the kinematic constraint that the circumferential velocities of the rotor and the inner-race of the back-up bearing at the contact point equal to each other. At the same time, if this solved friction force exceeds the maximum static friction force ($= \mu_s F_{nk}$), equation (3.b) applys again.

DISCUSSION OF RESULTS

The rotor is modeled with 34 stations (as shown in Fig. 1) and the first four modes (two rigid body and two flexible modes) are included in the simulation model. The two auxiliary bearings are located at nodes 3 and 33, respectively. This arrangement is taken to represent one of the most technically feasible configurations in that it greatly simplifies bearing maintenance. It is assumed that the two auxiliary bearings are identical in terms of stiffness, damping and friction characteristics. Some nominal system parameters used for the simulation study are K_C=2.855e+6, ξ=0.03, R_{mk}=1.1 R_{Bk}, μ_s=0.5 and μ_ψ=0.002. To avoid excessive cluttering of plots, all the results that are presented in this paper correspond to node 3, the location of bearing #1.

Since the total system which includes two bearings and associated friction forces as well as the inner–race motions is rather complicated and requires considerable amount of computer time for the solutions to converge, the friction effect is examined first to see if the model can be further simplified. It turns out that the steady–state results obtained with and without friction are virtually identical. Even the differences in transient responses are quite small, as can be seen in Fig. 3(a) and 3(b). The only remarkable effect is on the transient responses of the inner-race as shown in Fig. 3(c). This observation is confirmed by numerous runs using different system parameters and rotor speeds. The lack of significance of friction may be attributed to several factors. First, the inertia of the inner-race is quite small in comparison to the rotor mass, so vibration of the bearing has little influence on the rotor vibration. Second, ball bearings exhibit quite negligible torsional resistance under normal conditions. As a result, the terms that are related to the friction forces and the rotational motion of the inner race are not included in the simulations that are discussed in the following paragraphs.

The steady–state response characteristics of the system are obtained through numerical integration of the simplified version of governing equations (1) and (2). Near–zero initial conditions are used, simulating situations where the AMBs are functioning properly prior to a system failure. Multiple solutions with other initial conditions are not sought at present.

It is well known from linear analyses that imbalance greatly affects the steady state vibration amplitudes of a rotor system. However, it is observed from the current work that imbalance may also influence frequency content of the rotor responses quite dramatically at certain operating speeds. A typical case with such an imbalance effect is shown in Figs. 4 and 5, where orbits and corresponding frequency spectra of the rotor for different values of imbalance at the speed of $\Omega = 1000$ are plotted. For this particular case, there exist eight ranges of imbalance values that result in eight different types of rotor responses.

For $e \leq 0.0009$, the rotor rotates near the bottom of auxiliary bearings and the responses are predominantly synchronous (Figs. 4(a)-4(b) and 5(a)-5(b)). As imbalance increases, the 2Ω superharmonic component approaches the magnitude order of the synchronous component (Figs. 4(b) and 5(b)). However, the responses are of small amplitude. For $0.0010 \leq e \leq 0.0013$, the responses are dominated by $\Omega/2$ subharmonic components (Figs. 4(c) and 5(c)). In other words, the amplitude of $\Omega/2$ component is greater than that of the synchronous. For $0.0014 \leq e \leq 0.0016$, the $\Omega/2$ subharmonics disappear and the $\Omega/3$ subharmonics become dominant (Figs. 4(d) and 5(d)). So far, the overall amplitude of the responses are not large, the rotor just bounces near the bottom of the auxiliary bearings. For $0.0017 \leq e \leq 0.0027$, the orbits become chaotic-looking (Fig. 4(e)) and the spectrum contains a lot of noise (Fig. 5(e)). In this range of imbalance, the rotor changes from bouncing near the bottom to bouncing around the full clearance of the bearing as imbalance increases. In the middle of this transition range, true chaos is observed. The Poincare map shown in Fig. 6(a) and the frequency spectrum shown in Fig. 6(b) demonstrate that the response has all the characteristics of a chaotic phenomenon. It should be noted that even though the orbits are chaotic looking, the amplitudes are not the largest among all the cases for this particular parametric configuration. For $0.0028 \leq e \leq 0.0034$, the orbits orbits are no longer chaotic–looking (Fig. 4(f)). The spectrum shows they are $\Omega/5$ subharmonic responses (Fig. 5(f)). Notice the amplitudes are the largest for this parametric configuration. For $e = 0.0035$, the amplitude suddenly becomes smaller even though the imbalance has become larger (Fig. 4(g)). And the rotor bounces near the bottom of the auxiliary bearings again. The frequency spectrum shows it is $\Omega/8$ subharmonic response (Fig. 5(g)). For $0.0036 \leq e \leq 0.0042$, the orbits become chaotic-looking again (Fig. 4(h)). But the frequency spectra are very similar to the subharmonic cases (Fig. 5(h)), only with some discrete noise. Finally, for $e \geq 0.0043$, the responses become predominantly synchronous again (Figs. 4(i)-4(j) and 5(i)-5(j)). But this time as imbalance increases, the 2Ω superharmonic component become smaller and smaller (Figs. 4(j) and 5(j)).

Examining all the orbits in terms of amplitudes as imbalance increases, we can see the characteristics of a jump–type phenomenon (Cunningham, 1958). The jump–down takes place around $0.0034 < e < 0035$ where the rotor jumps

from full-clearance bouncing to near–bottom bouncing. Further investigation is needed to better understand this type of change.

Imbalance responses at some other operating speeds and for other parametric configurations exhibit similar changes as imbalance varies, though the imbalance ranges and corresponding response types may not be as well defined as in the above cases. In fact, subharmonic responses from $\Omega/2$ through $\Omega/10$ are all observed except $\Omega/9$ as shown in Figs. 7. Surprisingly, those subharmonics are not directly related to the system's natural frequencies as were the cases with other researchers' findings (such as Ehrich, 1988). Moreover, several types of subharmonic responses may occur at a single operating speed. It should be noted that Chen et al. (1993) also reported occurrence of three stable subharmonic responses at a single rotor speed in a SFD supported rotor system but did not provide any explanation for their findings. In their case, even the imbalance did not vary. Apparently, further research is needed to find a mechanism to explain this multi–subharmonic vibration phenomenon. On the other hand, it should be pointed out that these subharmonic responses are not typical cases. While some of them are observed to exist within a certain range of parameters, the majority of them occur only for some specific parametric configurations.

Due to space limitations, results for other parametric configurations are not systematically plotted. A general summation of the observations is presented instead. A common feature among all the responses is that for very small imbalance, the responses are always synchronous. The imbalance range that result in synchronous dominated responses depend on several system parameters. For small back-up bearing stiffness (such as K_B = 0.213e+6) and normal damping (C_B = 157.0), the responses are almost always synchronous. Only $\Omega/2$ subharmonic are observed at a few operating speeds with a very narrow range of imbalance. It should be noted that even though a lower K_B may leads to a better system response, it may also fail to protect the magnetic bearings due to the fact that it could result in a larger rotor orbit-center offset. However, the dramatic response changes discussed above may occur again if the damping becomes small (such as C_B = 57.0) even though the stiffness still remains small. On the other hand, increasing the damping C_B alone may not be able to eliminate those dramatic changes. It is observed that those changes can still occur for C_B being as large as 700.0. Reducing the size of clearance δ may not eliminate the response changes at certain speeds. But it can narrow the operating speed range where those changes occur. For example, response changes are eliminated for $\Omega \geq 1500$ when δ is reduced from 0.002 to 0.001 with all other parameters remaining the same, but response changes still occur for $\Omega \leq 1400$.

It is obvious that rotor responses involving nonsymmetric bearing clearance effect are very complex problems and numerical integration alone is not a sufficient tool to obtain a global picture of the system responses. The harmonic balance method is then used for the investigation of global system behavior. However, it is only attempted for situations with very small imbalance values. In addition, only the 1Ω harmonic is considered. The complex frequency contents associated with medium and large imbalance values makes it a formidable task to apply the harmonic balance method for other cases. Nevertheless, some useful information can be drawn from these results. After all, an adequately balanced rotor system should have very small imbalance under normal conditions.

Fig. 8(a) shows that nonsymmetric clearance effect is equivalent to asymmetric stiffness effect with regards to critical speeds. The clearance actually splits the first critical speed into two pseudo–critical speeds. In the X direction, the gravity force tends to keep the rotor in contact with the bearing at low operating speed. Thus, the apparent stiffness is almost the same as K_B and the pseudo-critical speed is nearly the same as the critical speed for the linear case ($\delta = 0$). But in the Y direction, the clearance results in a lower apparent stiffness and, consequently, an additional lower-value pseudo-critical speed. It is seen that several higher order additional pseudo-critical speeds are created in the operating speed range in addition to the 1st additional pseudo-critical speed. It is noted that the response in the X direction also departs from the linear case at high operating speed. This is because the imbalance force becomes dominant at high rotor speed which in turn makes the gravity force less significant and the clearance effect more important. Fig. 8(b) shows that changing the auxiliary bearing stiffness has little effect on the pseudo–critical speeds of the system. However, for a larger value of imbalance, a higher K_B does leads to a greater tendency of double–valued responses. In each direction, for either a stiffness increase or an imbalance increase, the 1st pseudo–critical peak tend to become a hard–spring type jump and the 2nd one tend to develop into a soft-spring type jump, with the tendency decreasing as the pseudo–critical's order increases.

Fig. 9(a) shows double–valued responses in the Y direction for four different values of clearance. It is seen that a larger clearance results in wider rotor speed range of double–valued responses. It is also observed that as clearance increases, the apparent stiffness decreases and the first pseudo–critical speed shifts to a lower value. Fig. 9(b) shows the double–valued responses in the X direction. Even though the jumps themselves are smaller in magnitude, they are more obvious in trend. Notice how little the change is for the first pseudo-

critical speed in the X direction.

Fig. 10(a) shows the influence of auxiliary bearing damping on the double–valued responses in the Y direction. It is observed that the damping has to be quite large to eliminate the double–valued responses associated with the first pseudo–critical speed. Fig. 10(b) shows the influence of C_B on the double–valued responses in the X direction. In both figures, it should be noted that as C_B decreases, the second pseudo–critical speed peak will develop into a soft–spring type jump and the third pseudo–critical speed peak will evolve into a hard–spring type jump.

The system behaviors for higher operating speed range are not shown in Figs. (9) and (10) so that the jump phenomena can be more clearly illustrated. It is also because that the system's responses at high operating speed range with the same parameters are more or less regular, in other words, mainly amplitude changes.

CONCLUSIONS

As a summary of the results discussed above, the following conclusions can be drawn:

1. Imbalance may change the rotor responses dramatically in terms of frequency contents at certain operating speeds, especially under conditions of large clearance, high bearing stiffness and low bearing damping. With imbalance changing, as many as eight different types of responses may occur for a particular parametric configuration at a single operating speed.
2. Subharmonic responses of second order through tenth order are all observed except for the ninth order case. However, the majority of them are not typical cases, and were observed only for quite particular parametric configurations.
3. Chaotic phenomenon is observed to occur occasionally. However, the amplitudes associated with such motion are not among the largest.
4. Nonsymmetric clearance effects influence the critical speeds in a manner similar to asymmetric stiffness effects.
5. Double–valued responses in the form of both hard-spring type jump and soft-spring type jump are observed to be possible at low operating speeds with low auxiliary bearing damping or high imbalance. With large clearances or high bearing stiffness, the jump phenomenon may occur for even relatively small imbalances.
6. The effect of friction between the shaft and the inner race of a rolling element auxiliary bearing on the dynamics of the rotor is quite small and can reasonably be neglected for steady–state analyses.

ACKNOWLEDGEMENT

The authors would like to express their gratitude to S. Klusman of Allison Gas Turbines, Inc. for many helpful discussions and practical advice.

This work was supported by NASA under Grant No. NAG3–1507. The Government has certain rights in this material.

REFERENCES

Bently, D. E., 1974, "Forced Subrotative Speed Dynamic Action of Rotating Machinery," ASME Paper No. 74-PET-16.

Black, H. F., 1968, "Interaction of a Whirling Rotor With a Vibrating Stator Across a Clearance Annulus," *Journal of Engineering Sci ence*, Vol. 10, No. 1, pp. 1-12.

Chen, P. Y. P, Hahn, E. J., and Wang, G. Y., 1993, "Subharmonic Oscillations in Squeeze Film Damped Rotor Bearing Systems Without Centralizing Springs," ASME Paper 93-GT-428.

Childs, D. W., 1979, "Rub-Induced Parametric Excitation in Rotors," ASME *Journal of Mechanical Design*, Vol. 101, pp. 640-644.

Childs, D. W., 1982, "Fractional-Frequency Rotor Motion Due to Nonsymmetric Clearance Effects," ASME *Journal of Engineering for Power*, Vol. 104, pp. 533-541.

Cunningham, W. J., 1958, *Introduction to Nonlinear Analysis*, McGraw-Hill Book Co., New York, NY.

Ehrich, F. F., 1966, "Subharmonic Vibration of Rotors in Bearing Clearance," ASME Paper 66-MD-1.

Ehrich, F. F., 1988, "High Order Subharmonic Response of High Speed Rotors in Bearing Clearance," ASME *Journal of Vibration, Acoustics, Stress, and Reliability in Design*, Vol. 110, pp. 9-16.

Ehrich, F. F., 1991, "Some Observations of Chaotic Vibration Phenomena in High-Speed Rotordynamics," ASME *Journal of Vibration, Acoustics, Stress, and Reliability in Design*, Vol. 113, pp. 50-57.

Gelin, A., Pugnet, J. M., and Hagopian, J. D., 1990, "Dynamic Behavior of Flexible Rotors with Active Magnetic Bearings on Safety Auxiliary Bearings," *Proceedings of 3rd International Conference on Rotordynamics*, Lyon, France, pp. 503-508.

Ishii, T., and Kirk, R. G., 1991, "Transient Response Technique Applied to Active Magnetic Bearing Machinery During Rotor Drop," *DE- Vol. 35, Rotating Machinery and Vehicle Dynamics, ASME*, pp.191-199.

Muszynska, A., 1984, "Partial Lateral Rotor to Stator Rubs, " IMechE Paper No. C281/84.

Yamamoto, T. T., 1954, "On Critical Speeds of a Shaft," *Memoirs of the Faculty of Engineering*, Nagoya University (Japan), Vol. 6, No. 2.

TABLE 1. FEM MODEL DATA

Station (in.)	O.D. (in.)	I.D. (in.)	WT. (lb)	Polar Mom. (lb.in.s^2)
5.400	2.800	2.000	0.000	0.000
5.450	2.800	2.000	5.000	5.000
6.500	2.800	2.000	0.000	0.000
6.505	7.300	6.950	0.100	0.100
7.100	7.300	6.950	0.000	0.000
8.670	7.300	7.120	30.400	425.000
10.900	8.400	8.220	0.000	0.000
13.120	9.300	9.120	0.000	0.000
15.310	10.100	9.920	20.300	538.000
17.280	10.700	10.550	9.150	302.000
18.580	11.200	11.050	0.000	0.000
19.880	11.550	11.400	0.000	0.000
21.120	11.950	11.800	0.000	0.000
22.380	12.150	12.000	41.900	1645.000
23.670	12.400	12.250	0.000	0.000
24.900	12.500	12.350	0.000	0.000
26.120	12.500	12.350	0.000	0.000
27.400	12.500	12.350	22.550	539.000
27.750	12.500	2.500	1.027	0.000
27.800	4.500	2.500	7.733	0.000
32.000	4.500	2.500	25.022	49.761
37.000	4.500	2.500	17.961	0.000
43.000	4.500	2.500	17.961	0.000
48.000	4.500	2.500	16.328	0.000
53.000	4.500	2.500	16.328	0.000
58.000	4.500	2.500	14.614	0.000
61.950	4.500	2.500	6.531	0.000
62.000	6.000	2.500	0.954	0.000
62.405	6.000	5.670	34.935	1216.500
64.600	6.000	5.670	0.000	0.000
67.000	6.000	5.670	117.000	3750.500
69.500	6.000	5.670	0.000	0.000
69.505	2.850	1.250	0.000	0.000
72.500	2.850	1.250	10.197	12.000
73.600	2.850	1.250	0.000	0.000

Modulus of elasticity: E=2.80e+7 psi
Shear Modulus of elasticity: G=1.08e+7 psi

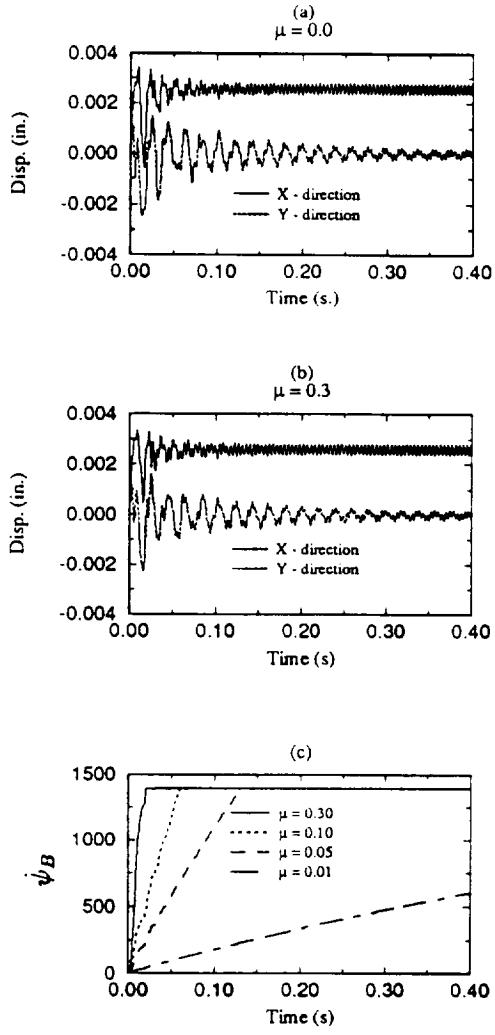

FIG. 3 EFFECTS OF BEARING FRICTION (C_B=157.0, K_B=0.313e+6, Ω=1400, δ=0.002, e=0.0002)

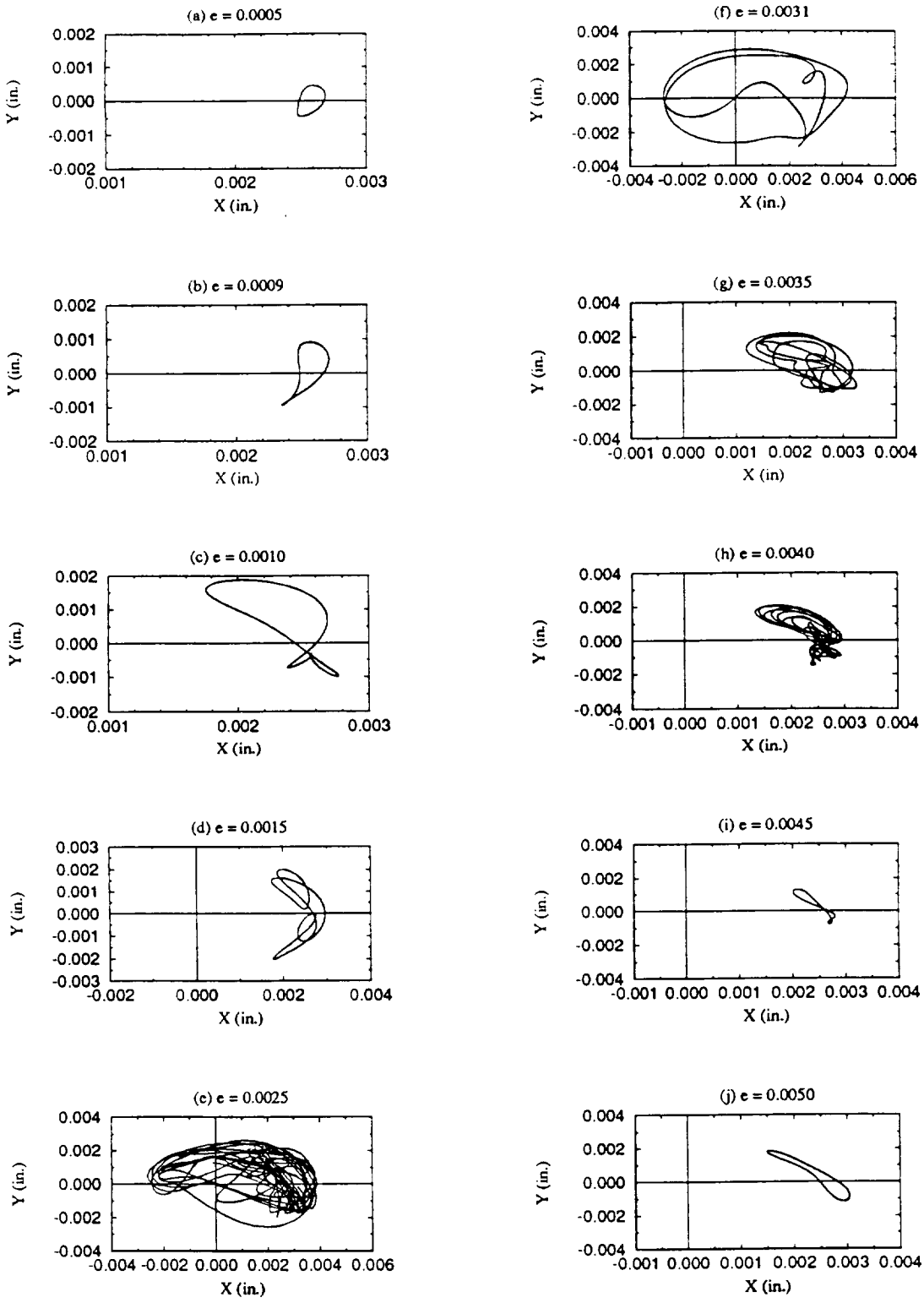

FIG. 4 IMBALANCE RESPONSES - ORBITS
(δ=0.002, K_B=0.313e+6, C_B=157.0)

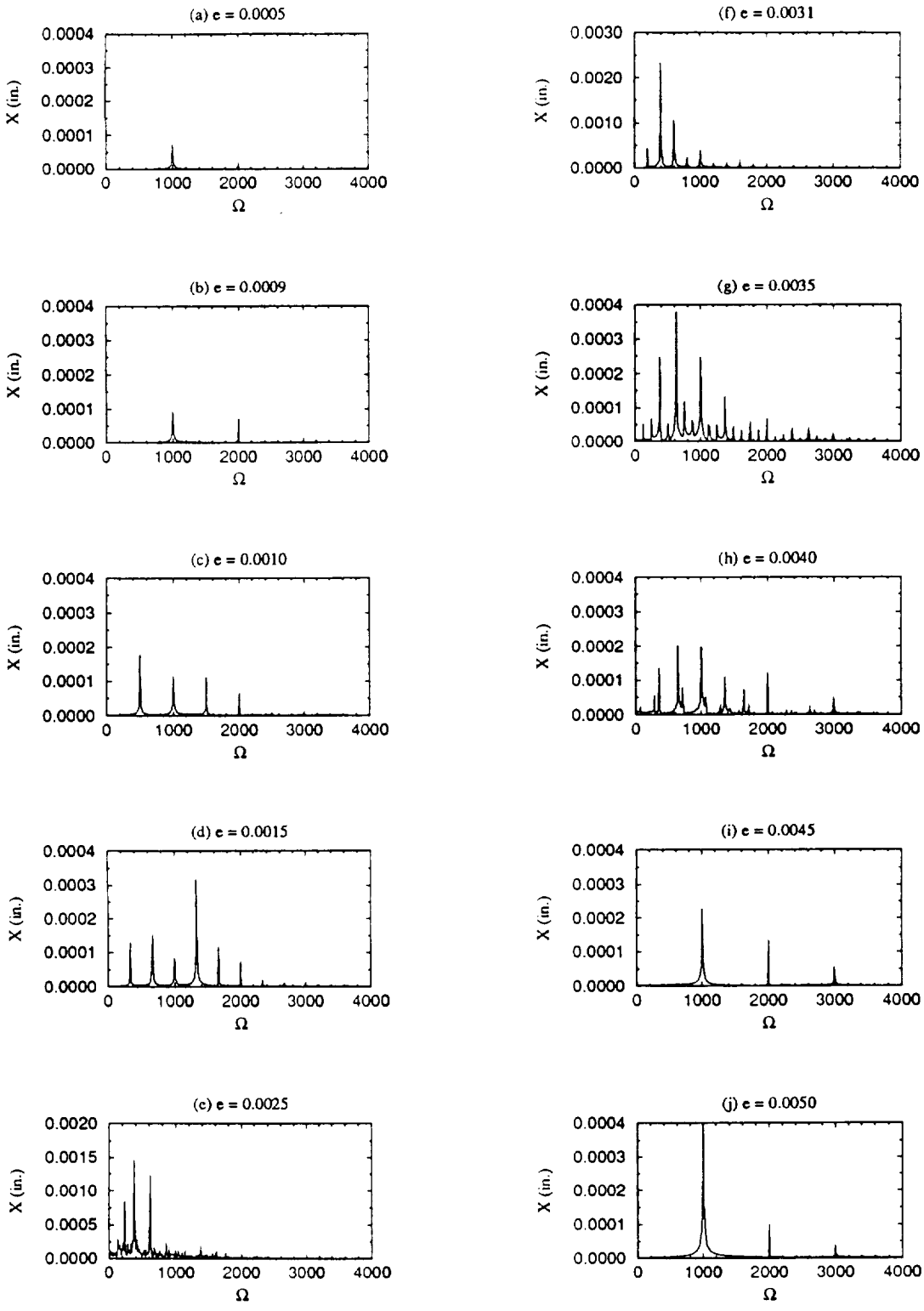

FIG. 5 IMBALANCE RESPONSES - SPECTRA
(δ=0.002, K_B=0.313e+6, C_B=157.0)

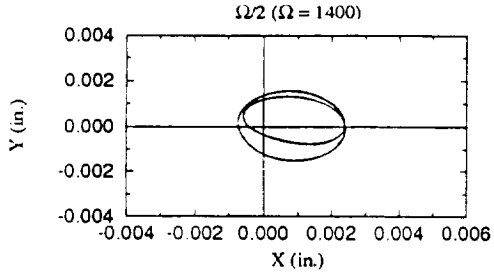

(a) δ=0.001, e=0.0007, C_B=157.0,

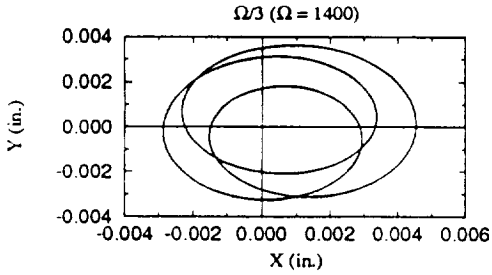

(b) δ=0.001, e=0.0029, C_B=157.0,

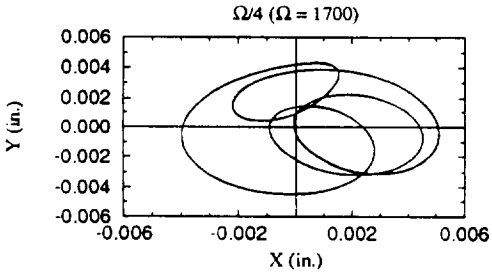

(c) δ=0.002, e=0.00105, C_B=145.0,

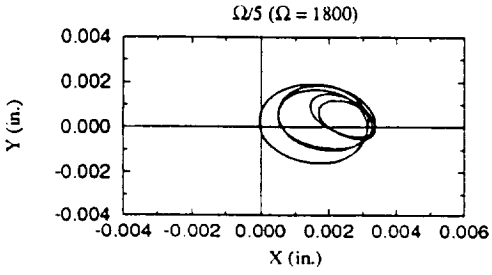

(d) δ=0.002, e=0.00067, C_B=157.0,

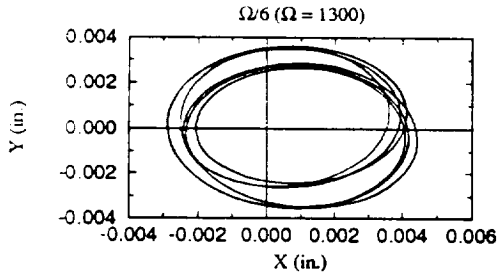

(e) δ=0.002, e=0.0025, C_B=157.0,

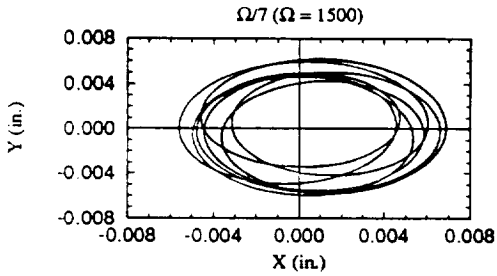

(f) δ=0.002, e=0.0032, C_B=157.0,

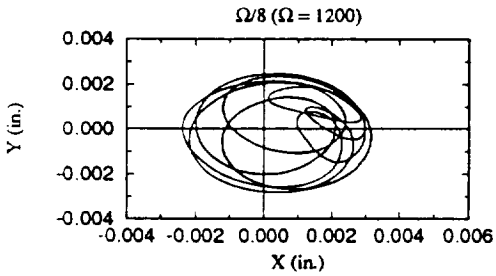

(g) δ=0.001, e=0.0030, C_B=157.0,

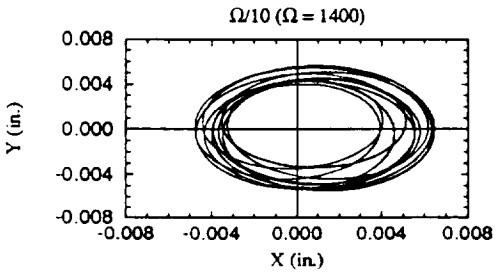

(h) δ=0.002, e=0.00395, C_B=157.0,

FIG. 7 SUBHARMONIC RESPONSES (ORBITS)
(K_B=0.313e+6)

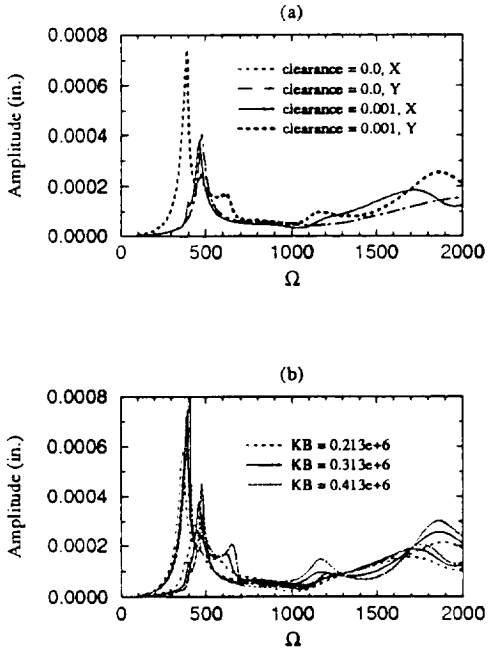

FIG. 8 INFLUENCE ON CRITICAL SPEEDS
(a) e=0.0001, C_B=157.0, K_B=0.313e+6
(b) e=0.0001, C_B=157.0, δ=0.001

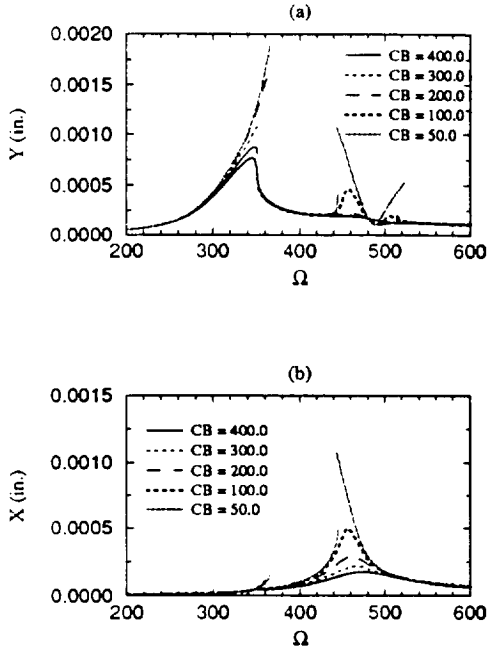

FIG. 10 EFFECTS OF BACK-UP BEARING DAMPING
(δ=0.002, e=0.0001, K_B=0.313e+6)

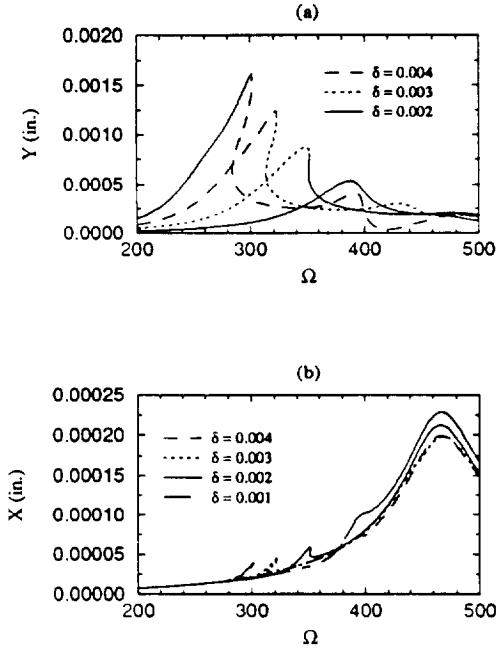

FIG. 9 CLEARANCE EFFECT ON JUMP PHENOMENA
(e=0.0001, K_B=0.313e+6, C_B=300.0)

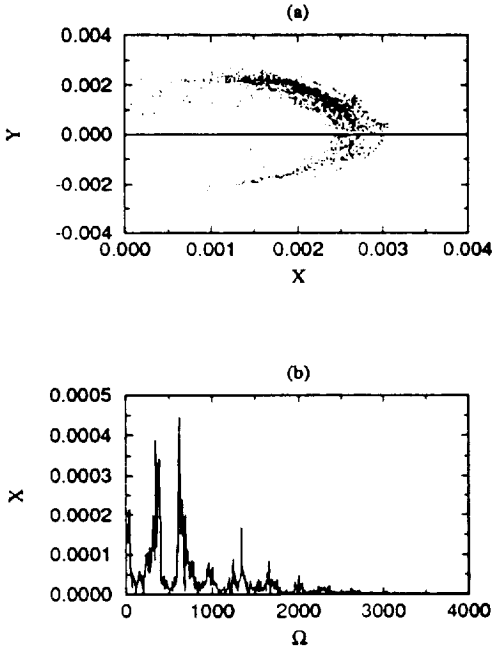

FIG. 6 CHAOTIC RESPONSES (e = 0.0023,
δ=0.002, K_B=0.313e+6, C_B=157.0)

OMIT

TSI Press Series

FIRST INDUSTRY/ACADEMY SYMPOSIUM ON RESEARCH FOR FUTURE SUPERSONIC AND HYPERSONIC VEHICLES

Applications, Design, Development, and Research

Held December 4-6, 1994 in Greensboro, North Carolina, U.S.A.

Volume 1

Editors:

Abdollah Homaifar
Department of Electrical Engineering
North Carolina A&T State University

John C. Kelly, Jr.
Department of Electrical Engineering
North Carolina A&T State Unversity

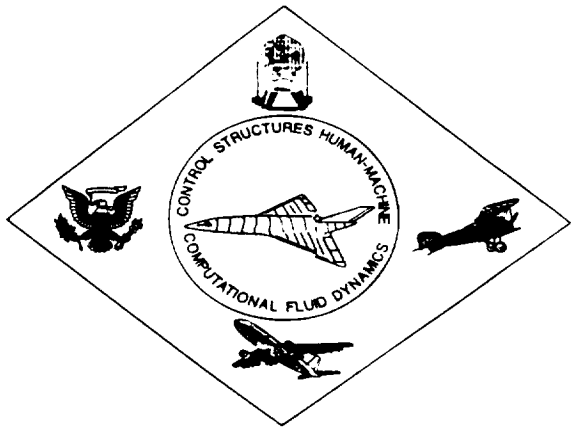

TSI Press Albuquerque, New Mexico USA 1994